Analytical Methods

PAPER

Check for updates

Cryogenically induced signal enhancement of Raman spectra of porphyrin molecules

Aria Vitkova, [ID] Scott J. I. Walker and Hanna Sykulska-Lawrence*

Raman spectroscopy is a powerful analytical technique in contemporary medicine and biomedical research due to its exceptional ability to provide an unambiguous spectroscopic signature of the molecular chemical composition, structure and atom arrangements. Among other applications, investigations of the Raman spectra of porphyrins and their derivatives have been critical in the study of ligand binding mechanisms and drug interactions with healthy and diseased blood cells, as well as for the analysis of blood, hemoproteins and the oxygenation process of human erythrocyte. However, obtaining Raman spectra with satisfactory definition of porphyrin-based molecules can be challenging due to their inherent photo- and thermal sensitivity which leads to laser damage even at low laser power. This severely affects the Raman spectra of porphyrins and limits the Raman signal strength and spectra quality. In this study, we examine two important porphyrins, hemin and protoporphyrin IX, at cryogenic temperatures down to 77 K using a 532 nm excitation Raman instrument in order to study the Raman signal strength and spectral quality dependence on the sample temperature at these extreme low temperatures. We report a significant Raman signal enhancement of up to 310% in the spectra at cryogenic temperatures compared to room temperature measurements. This provides a remarkable improvement of the quality and definition within the spectra and demonstrates that cryogenic Raman measurements can be used as an exceptionally effective method of enhancing the Raman signal and spectra quality for investigations of porphyrins and their derivatives regardless of the excitation wavelength selection. This can greatly improve the effectiveness of Raman spectroscopy in biomedical research, especially in the field of drug design and development, medical diagnostics and disease monitoring and analysis.

Introduction

The structure and function of porphyrins and porphyrin derivatives is intensively studied in contemporary medicine and analytical biochemistry research due to the critical role of these compounds in many biological processes. Raman spectroscopy has gained popularity in the analysis of the structural properties and functions of porphyrin complexes as well as many other biological molecules due to its exceptional ability to unambiguously differentiate between different chemical structures and atom arrangements within molecules, even in molecules of the same chemical composition. This provides a highly specific spectroscopic fingerprint that can be used to identify and study changes in the molecular structure and coordinates of porphyrin molecules and thus characterize their function within biological processes. This has been extensively used to provide critical information in medicine and drug development research.

Besides many other applications, Raman spectroscopic investigations of porphyrins and their derivatives have been critical in the study of ligand binding mechanisms,[1–3] hemoglobin and whole blood analysis for monitoring pathological changes in biomedical analysis and diagnostics[4–7] or observations of the oxygenation process of human erythrocyte.[7–9] The Raman spectra of porphyrin based molecules have also been used to study healthy and diseased blood cells in order to investigate drug interactions with cells infected by malaria[7,10–12] and for the analysis of sickle cells in sickle cell disease research.[7,8,10] Additionally, the potential for early detection of malaria infection has also been demonstrated.[7,13,14]

However, obtaining Raman spectra with adequate definition of porphyrins and their derivatives can be challenging due to their inherent photo- and thermal sensitivity leading to photo-induced and thermal damage under laser light exposure. The laser damage can severely affect the Raman spectra and the effectiveness of the Raman method in biomedical research.[8,9,15,16] It also limits the laser power that can be applied which significantly reduces the resulting Raman signal strength and thus limits the definition within the spectra, which may be critical for many applications.[9,15,16] As such, obtaining Raman spectra of porphyrin complexes without photodamage requires the careful selection of the laser power and excitation wavelength.

Astronautics Research Group, University of Southampton, Southampton, SO17 1BJ, UK. E-mail: H.M.Sykulska-Lawrence@soton.ac.uk; Tel: +44 (0)2380 592313

The effects of the excitation wavelength and different Raman methods and configurations on the spectra of porphyrins and porphyrin derivatives have been previously studied to characterize the Raman resonance effects and mechanisms leading to signal enhancement.[4–6] Whole blood and hemoproteins have been analysed using Fourier transform Raman spectroscopy (FT-R) at the near infrared (NIR) excitation of 1064 nm, which was suggested to reduce the sample damage effects.[5] However, Raman scattering in the NIR range is much weaker than Raman scattering in the visible. The Raman signal is inversely proportional to the 4th power of the incident light wavelength and other studies of the Raman spectra of porphyrin derivatives indicate that the 1064 nm excitation provides only very weak Raman spectra compared to other traditionally used excitation wavelengths.[4,12,17] A study of whole blood and hemoglobin at visible excitation (514.5 nm) and NIR excitation (720 and 1064 nm) suggests that excitation at 720 nm is more practical for *in vivo* measurements than visible or 1064 nm excitation as it can still benefit from resonance effects and yield satisfactory Raman spectra while avoiding fluorescence and carotenoid interference which occurs at visible excitations.[4,17]

A study of the Raman band vibrational mode assignments and the impact of the excitation wavelength selection on the Raman spectra signal enhancement of β-hematin and hemin has been conducted and shows promising signal enhancement at 780–830 nm as well as at 564 nm excitation.[12] However, it also shows that the signal enhancement using resonance at these excitation wavelengths is very specific to individual vibrational modes and Raman bands.[12] Depending on the application, selecting a different excitation for signal enhancement may also not be a viable option as in some cases, certain spectral features may be only observable at specific excitations, or due to interference from other molecules and fluorescence.[4,5,7,12,14–16]

Research conducted at 632.8 nm between 4 °C and 52 °C (277 K and 325 K) indicates that limiting the exposure to laser light, as well as performing measurements at lower temperatures (277 K), reduces the photo- and thermal damage and also results in a higher quality Raman spectra of the porphyrin-based molecules.[8] While limiting the laser light exposure reduces the damage but also the Raman signal strength, reducing the temperature could be an effective non-invasive method of enhancing the signal without any negative side-effects. However, Raman spectra are routinely obtained at room temperatures (15–25 °C, 288–298 K) and there has been limited research into the effect of low temperatures on the Raman spectra of porphyrin molecules and its potential of enhancing the Raman signal.[18] Raman spectra of some other organic molecules have been observed at cryogenic temperatures reporting a wide variety of thermally induced changes.[19–26] These changes have proven very molecule specific and as such, a dedicated study of porphyrins at cryogenic temperatures is necessary to confirm the thermally induced changes in their Raman spectra.

In this study, we examine two important porphyrins, hemin and protoporphyrin IX, at cryogenic temperatures ranging down to 77 K using Raman spectroscopy at 532 nm excitation in order to study the Raman signal strength and spectral quality dependence on the sample temperature at these extreme conditions. We report a significant Raman signal enhancement at cryogenic temperatures compared to Raman spectra obtained at room temperature, which may provide better resolution and definition within the spectra regardless of the excitation wavelength selection and thus improve the effectiveness of Raman spectroscopy in biomedical research.
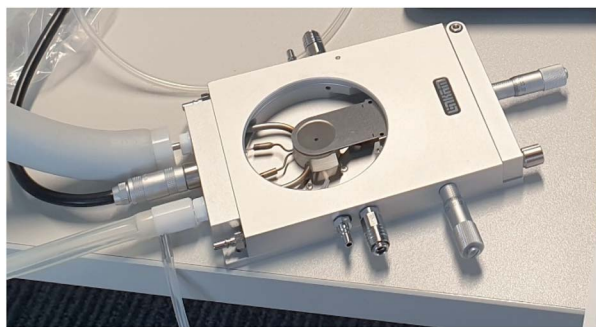
Experimental

In this study, two important porphyrins, hemin and protoporphyrin IX, were examined at cryogenic temperatures (173 K and 77 K) and at room temperature (here 295 K) at various laser power setting using a 532 nm excitation Raman InVia Renishaw spectrometer. The nominal laser power of the Raman system is 44.9 mW (195.4 kW cm^{-2} power density) and the sample exposure time 120 s with the sample laser power density in the ranges 1.95 to 97.7 kW cm^{-2} and 0.195 W cm^{-2} to 9.77 kW cm^{-2} used to obtain the Raman spectra of hemin and protoporphyrin IX, respectively. The 532 nm excitation wavelength is one of the most widely used Raman excitation wavelengths that is standard in the industry and commonly used for similar applications. The sample spot size used for the measurements was 5.41 μm in diameter and the spectral resolution of the system is 0.7 cm^{-1} to 0.3 cm^{-1} (using the full width half maximum method, *i.e.* FWHM).

The porphyrin samples were selected to represent important porphyrins and precursors for many applications in medicine, biomedical research and drug development. Both samples, hemin (Alfa Aesar, >97% purity) and protoporphyrin IX (PorphyChem, >98% purity), were examined in their powder form with a layer thickness of approximately 0.5 mm. The powder form was selected to observe the cryogenically induced changes without introducing additional variables in the form of concentration levels and molecular interactions with different solvents. This is specific to each application and can be explored in future experiments.

The samples were cooled to cryogenic temperatures using a Linkam THMS600 liquid nitrogen cooling system, which is a standard temperature-controlled stage widely used for Raman measurements and is shown in Fig. 1. The cooling rate was 55 K min^{-1} and a 6 minutes dwell time was applied after reaching the required measurement temperature to ensure the temperature of the sample is equilibrated. An initial sweep of measurements across different laser powers was performed in an ambient environment to identify the most suitable power density setting for the measurements at cryogenic temperatures. Subsequently, 3 measurements at each temperature setting (295 K, 173 K and 77 K) at the most suitable power density setting were performed in a nitrogen purged environment using the Linkam cooling system. It is important to note that liquid nitrogen Raman spectra is characteristic of a single very strong peak at 2327 cm^{-1}, which is outside of the porphyrin Raman signature range. As such, nitrogen Raman signature generated by the nitrogen purged environment within the stage does not have any impact on the measurements and does not interfere with the spectra of porphyrins.

Fig. 1 An open Linkam THMS600 cooling stage showing the cooling block used for the experiments. The stage is closed and purged with liquid nitrogen *via* the liquid nitrogen tubes on the left-hand side. A temperature controller is connected to the stage and a PC interface software, which is used to set the temperature profile.

In order to avoid cumulative sample degradation, each measurement was performed at a different location within the sample. The impact of the variation between sample locations and the number of molecules measured by each spectra acquisition as well as the general variance in the measurements due to experimental error was evaluated by the σ error bar analysis, which did not reveal any excessive variance in the data.

All measurements were performed in the dark in a background light blocking cage and a galactic ray removal was applied to avoid interference. No other postprocessing was applied to the data before plotting the spectra.

The resulting spectra are shown and characterized and a comparison at different temperatures and laser power settings is provided. Peak fitting and FWHM were used for the identification of the Raman bands and the signal intensity. In order to assess the signal enhancement within the spectra, a signal to noise ratio (SNR) was calculated for all dominant Raman peaks in the spectra. The absolute intensity of the peaks and a noise reading at an adjacent valley in the spectra were used for the SNR calculation in order to avoid any fluorescence or background noise irrelevant to the signal enhancement affecting the SNR data.

An optimized density functional theory (DFT) vibrational frequency calculation was run using split valence polarization (SVP) together with polarizability calculations in order determine theoretical Raman vibrational frequencies and Raman activity of the two porphyrin molecules. These calculations were then used to assign vibrational modes to the Raman peaks within the spectra in order to provide further information on the character of the cryogenically induced changes.

Results and discussion

Both hemin and protoporphyrin IX were examined using the same 532 nm Raman system at various laser power settings in order to identify the optimal laser power that would allow acquisition of the highest quality Raman spectra achievable with this system at room temperature.

Fig. 2 shows the spectra of both porphyrins obtained at the optimal laser power density (9.77 kW cm^{-2} for hemin and
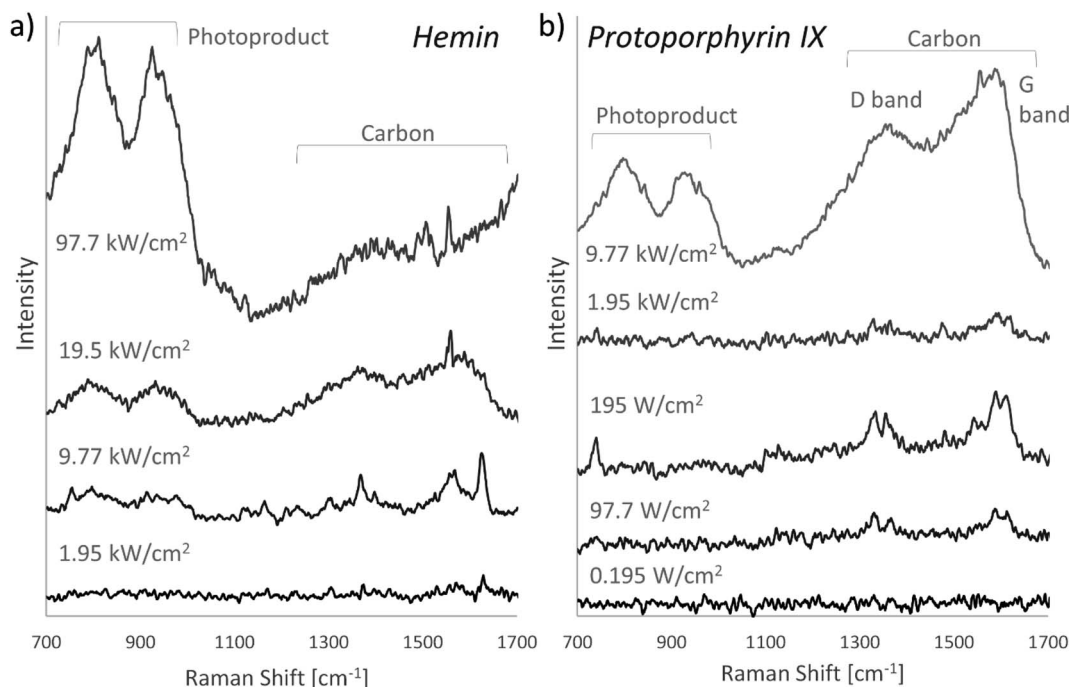
Fig. 2 Raman spectra of hemin (a) and protoporphyrin IX (b) at 532 nm excitation across different laser power settings at room temperature (295 K, 22 °C) showing the optimal Raman spectra at 9.77 kW cm^{-2} for hemin and 195 W cm^{-2} for protoporphyrin compared to spectra obtained at lower and higher laser power (note: spectra shown in this figure are vertically offset for clarity).
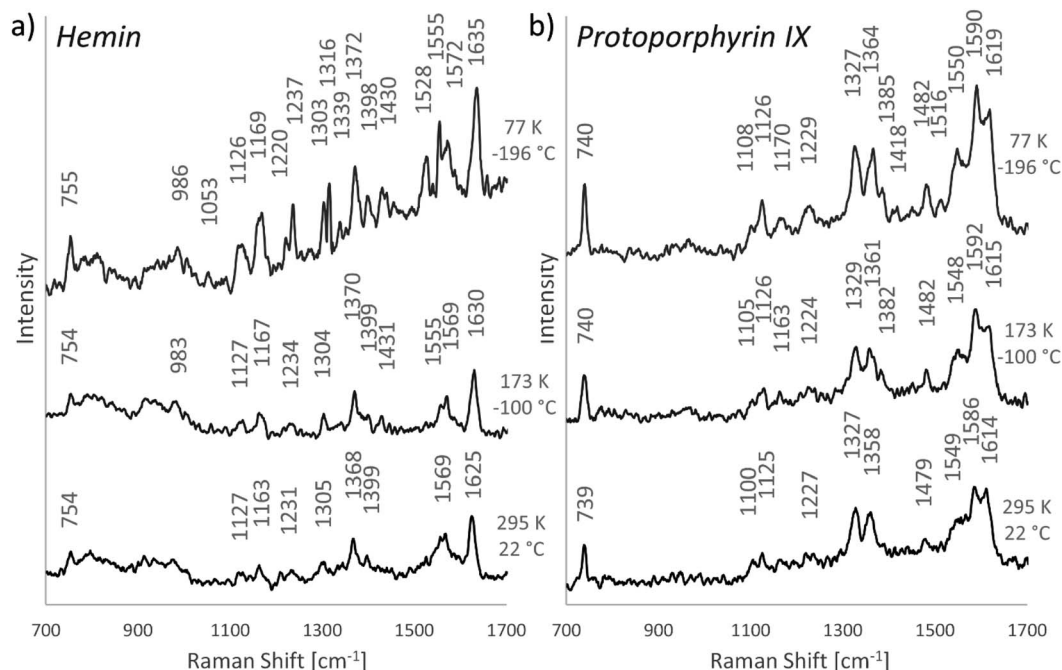
Fig. 3 The comparison of the Raman spectra of hemin (a) and protoporphyrin IX (b) in a nitrogen purged environment at cryogenic temperatures (173 K and 77 K) and room temperature measurements using 532 nm excitation and the same laser power density of 9.77 kW cm^{-2} for hemin and 195 W cm^{-2} for protoporphyrin (note: spectra shown in this figure are vertically offset for clarity).

195 W cm^{-2} for protoporphyrin IX) compared to spectra obtained at lower and higher power density settings. The spectra displayed in the figure demonstrate that only a relatively small change in the power of the incident laser beam can severely affect the Raman signal in terms of the signal strength, definition and occurrence of sample degradation signs. As shown in Fig. 2, while a spectral signature of hemin can be distinguished in the spectra obtained at 9.77 kW cm^{-2}, the signal progressively decreases until it is barely resolvable at 1.95 kW cm^{-2} with no signal at all returned at any lower power setting. On the other hand, the intensity of the hemin spectral signature also decreases above the 9.77 kW cm^{-2} power density and becomes increasingly overshadowed by the Raman signature of photodegradation products due to sample damage. Even at a relatively small increment of 2.24 mW laser power increase (i.e. 9.73 kW cm^{-2} power density), the hemin signal is no longer observable within the carbon signature in the spectra induced by sample thermal degradation.

Protoporphyrin shows even higher levels of photosensitivity as significant signal decrease due to sample degradation is observable even at a laser power density just above the optimal 195 W cm^{-2} power density setting until the signal becomes essentially unresolvable at 1.95 kW cm^{-2}.

Furthermore, even at the optimal power density, the Raman spectra of both hemin and protoporphyrin collected at room temperature lack the spectral definition necessary for full analysis and would not be satisfactory for many applications in biomedical research. Only a very weak low-definition Raman spectra of hemin can be obtained at these conditions and the spectra of protoporphyrin only shows its most dominant Raman bands. This may be partly due to the 532 nm excitation wavelength not being ideally suited for the detection of porphyrins.

However, as shown in Fig. 3, a substantial improvement in the spectral definition and signal strength can be observed at cryogenic temperatures at the same laser power density setting.

As displayed in Fig. 3, the Raman spectra of hemin obtained at 77 K shows a remarkable signal enhancement compared to the spectra obtained at room temperature. Some bands, namely 983 cm^{-1}, 1220 cm^{-1}, 1339 cm^{-1}, 1431 cm^{-1} and 1555 cm^{-1}, that are not visible at all at room temperature, become more distinguishable at 173 K and then clearly resolvable at 77 K. Additionally, strong Raman bands at 1303 cm^{-1} and 1528 cm^{-1} that are not observable at all at 295 K nor 173 K appear remarkably strong and well defined at 77 K.

While the occurrence of previously unresolvable bands and signal increase are not as dramatic as in the spectra of hemin, the spectra of protoporphyrin at cryogenic temperatures also shows a significant signal enhancement and much higher spectral definition. Previously unresolvable bands at 1163 cm^{-1} and 1382 cm^{-1} become distinguishable at 173 K and another minor band at 1418 cm^{-1} appears in the spectra at 77 K.

It is important to note that all Raman bands displayed in the spectra of both porphyrins in Fig. 3 at all temperature settings are associated with normal modes as external vibrational modes associated with low-energy phonos do not appear in the spectral region evaluated in this study.

There are two separate factors that may be contributing to the observed photodegradation in the spectra, photochemical and photothermal degradation. Photochemical degradation in organic samples often stems from photooxidation and would

thus be mitigated in a vacuum or nitrogen purged environment. However, the mitigation of photochemical degradation in nitrogen purged environment such as applied in the cryogenic experiments does not explain the Raman signal increase at 77 K compared to room temperature and 173 K as all three experiments were carried out in a nitrogen purged environment. Spectra collected in ambient environment at various laser power (shown in Fig. 2) also do not show any significant difference compared to spectra collected at the same laser power in nitrogen purged environment (Fig. 3). As such, it is unlikely that the signal increase at cryogenic temperatures is the result of limiting the photochemical degradation.

On the contrary, photothermal degradation is directly associated with localized heat build-up, which can be mitigated or prevented by providing a heat sink. Previous studies have successfully reduced the photothermal degradation by mixing the pure porphyrin sample with a KBr at 1% concentration and pressing into a pellet, which acts as a heat sink.[27] In this experiment, the heat sink is provided by the Linkam cooling stage, which reduces the sample temperature to cryogenic levels and thus limits the photothermal degradation. As the results do not indicate any contribution of photochemical degradation reduction to the signal enhancement, it is reasonable to assume that the observed effect can be entirely assigned to the reduction in photothermal degradation.

It is also important to note that mixing porphyrin samples with KBr and pressing into a pellet may not be feasible for all applications, while reducing the temperature of the sample is a relatively simple and non-invasive experimental method of decreasing the photothermal degradation. Furthermore, mixing with KBr and pressing into a pellet as previously reported and reducing the temperature to cryogenic levels are not mutually exclusive methods and could be used in conjunction to achieve higher signal enhancement levels. While this is not within the scope of this study, it could be explored in future experiments as an additional avenue to further enhance the Raman signal of porphyrin molecules.

Table 1 Raman band assignments for hemin and protoporphyrin IX based on DFT calculation using SVP and polarizability functions for the calculation of Raman vibrational frequencies and Raman activity

Protoporphyrin IX				Hemin			
Raman band frequency (cm^{-1})				Raman band frequency (cm^{-1})			
RT	173 K	77 K	Assignment	RT	173 K	77 K	Assignment
739	740	740	C1–C20═N1–C17═C16 symmetrical stretch, C32–C33–C34 scissoring/rock	754	754	755	CH (1) rock, CH$_2$ (21) rock, OH (1) rock
1100	1105	1108	CH + CH$_2$ + CH$_3$ rock		983	986	CH$_2$ (27) rock, CH$_2$ (30) twist, CH$_3$ (25, 28) rock, CH (29, 26) rock
1125	1126	1126	Ring asymmetric stretching, CH + CH$_2$ + CH$_3$ rock			1053	CH$_3$ + CH$_2$ + CH rock
	1163	1170	CH + CH$_2$ + CH$_3$ rock, ring asymmetric stretching	1127	1127	1126	N1 ring asymmetric stretch, CH$_3$ wag (24, 25), CH (1, 16) rock
1227	1224	1229	CH$_2$ (32) rock, CH$_2$ (33) wag, CH rock	1163	1167	1169	CH$_2$ (21) twist H–O1–C23 scissoring, CH$_2$ (22) wag
1327	1329	1327	CH$_3$ (30, 31) wag			1220	CH rock, ring asymmetric stretching (N1, N3, N4)
1358	1361	1364	CH + CH$_2$ + CH$_3$ rock	1231	1234	1237	CH$_2$ (30) rock, CH rock
	1382	1385	CH$_2$ (21, 22) rock, CH$_3$ scissoring	1305	1304	1303	Ring asymmetric stretching, CH + CH$_2$ + CH$_3$ rock
		1418	Ring asymmetric stretching			1316	CH rock, CH$_3$ wag, CH$_2$ wag
1479	1482	1482	N4 ring asymmetric stretching, CH$_2$ (26) scissoring, CH$_3$ (27) twist			1339	CH$_3$ (24) wag
		1516	C9═C8 stretching, C28═C29 stretching, CH$_2$ (29) scissoring, CH$_3$ (30) scissoring	1368	1370	1372	CH$_3$ wag, CH$_2$ wag/scissoring, ring asymmetric stretching (N1, N2)
1549	1548	1550	C18═C19 stretching, C5═C6 stretching, C12–C11 stretching	1399	1399	1398	CH$_3$ wag, CH$_2$ scissoring, ring asymmetric stretching (N3, N4)
1586	1592	1590	C28═C29 stretching, CH$_2$ (29) scissoring, C9═C8 stretching		1431	1430	Ring asymmetric stretching (N3, N4), CH$_3$ twist, CH$_2$ (27) scissoring
1614	1615	1619	C26═C25 stretching, CH$_2$ (26) scissoring, C14–C13═C12 symmetrical stretching			1528	C13═C14 + C8═C9 stretching, CH$_3$ twist, CH$_2$ scissoring
					1555	1555	Ring asymmetric stretching (N1, N3, N4), CH$_3$ (24, 25, 28) twist, CH$_2$ (30) scissoring
				1569	1569	1572	C27═C26 stretch, CH (27) scissoring, CH (26) rock, C15═C16 scissoring
				1625	1630	1635	C29═C30 stretch, CH$_2$ (30) scissoring, CH (29) rock, CH rock, ring asymmetric stretching

It is also important to note that changes in the Raman band frequency were recorded at cryogenic temperatures due to the thermally induced changes in the molecular vibrations. This is reflected in Fig. 3. In the spectra of hemin, frequency changes from 0.32 cm^{-1} up to 4.71 cm^{-1} were recorded at 173 K and from 0.61 cm^{-1} up to 11.26 cm^{-1} at 77 K. In the spectra of protoporphyrin, changes in the band frequency from room temperature to 173 K were between 0.54 cm^{-1} and 6.28 cm^{-1}, and from room temperature to 77 K between 0.23 cm^{-1} and 7.32 cm^{-1}.

While frequency shifts to higher frequencies at low temperatures would be expected due to the increased rigidity of molecular bonds causing higher frequency vibrations, frequency shifts to lower frequencies have also been recorded. However, this may be due to the low quality of the spectra of both porphyrins at room temperature, which may have lacked the necessary definition to accurately determine the Raman band frequency.

While these changes are not negligible and can potentially confuse the analysis of the data if a database of spectra collected at much higher temperatures is used, they are also consistent and easily measurable. As such, they can be easily accounted for in the data analysis without affecting the final results.

The assignments of each Raman band observed in the spectra of both porphyrins is provided in Table 1 with the molecular structure displayed in Fig. 4. The majority of new bands that only became distinguishable in the spectra at cryogenic temperatures were associated with vibrational modes including the vibrations of CH$_3$ and CH$_2$ groups, particularly bending modes (rocking, wagging, scissoring or twisting). Additionally, Raman bands that shifted to higher frequencies by the largest amount were predominantly associated with vibrations in the outside chains and groups of the molecule. On the other hand, bands that shifted to lower frequencies or stayed relatively stable over the temperature range were at least partially assigned to ring stretching modes and other stretching modes within the molecule's main structure.

The SNR comparison at each temperature and each Raman band in Fig. 5 and 6 shows that the signal enhancement is specific to each band in the spectra of both hemin and protoporphyrin. Specifically, the most dominant Raman bands that are clearly visible in the spectra even at room temperature (such as 1625 cm^{-1}, 1569 cm^{-1} and 1368 cm^{-1} in the hemin spectra and 1614 cm^{-1}, 1358 cm^{-1} and 1327 cm^{-1} in the protoporphyrin spectra) showed much lower SNR increase at cryogenic temperatures than bands that were either not resolvable at all, or only appeared very weak in the room temperature spectra.
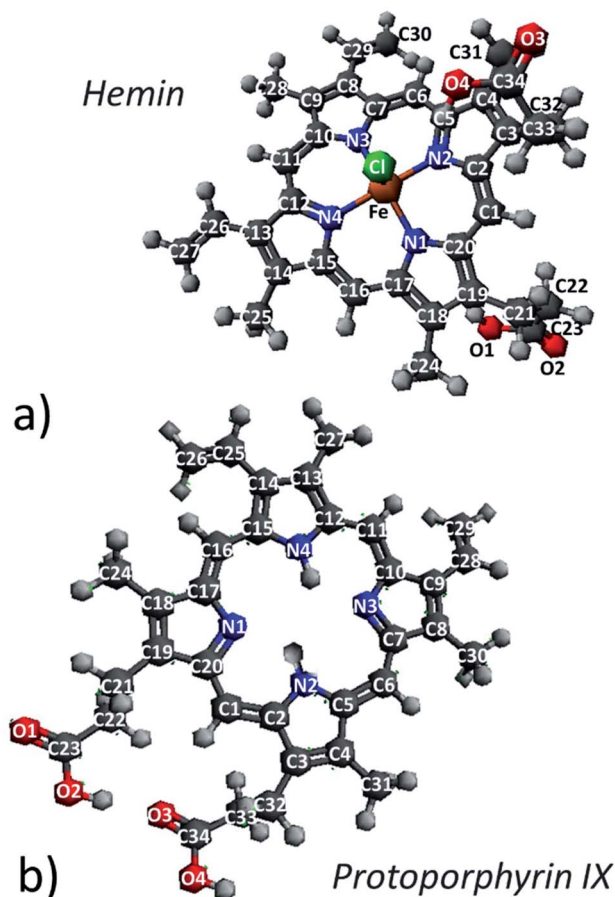

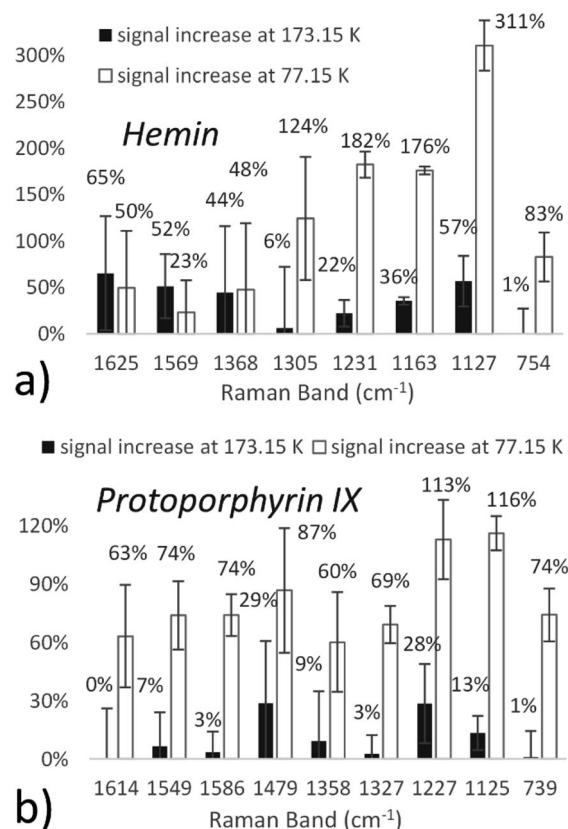Fig. 4 Molecular structure of hemin (a) and protoporphyrin IX (b).

Fig. 5 Relative SNR enhancement across all fully resolvable bands in the Raman spectra of hemin (a) and protoporphyrin IX (b) at cryogenic temperatures (173 K and 77 K) compared to room temperature measurements quantified in percentage of the nominal room temperature signal strength including 2σ error bars (532 nm excitation at 9.77 kW cm^{-2} laser power density for hemin and 195 W cm^{-2} for protoporphyrin).
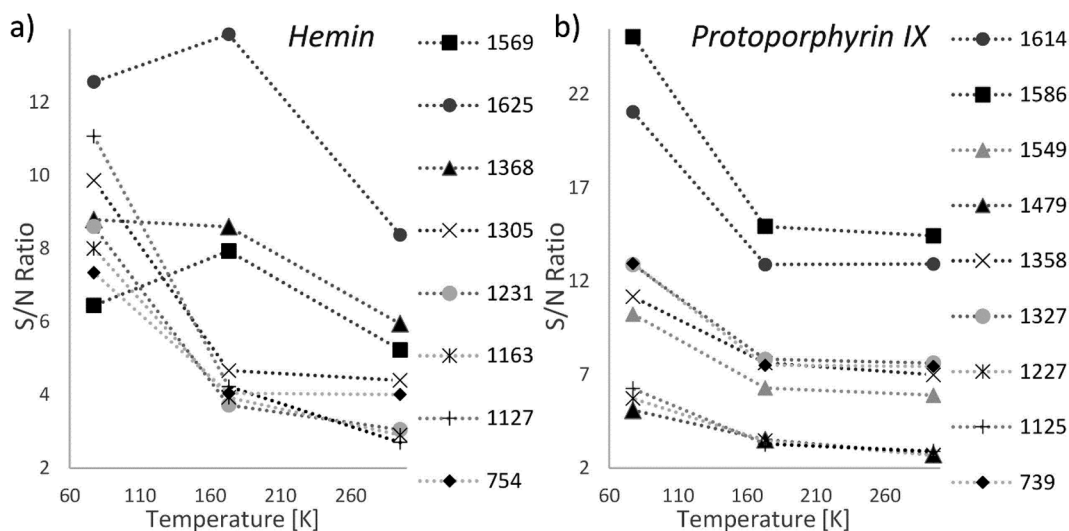
Fig. 6 SNR enhancement across all fully resolvable bands in the Raman spectra of hemin (a) and protoporphyrin IX (b) at cryogenic temperatures (173 K and 77 K) compared to room temperature measurements using 532 nm excitation and the same laser power density of 9.77 kW cm^{-2} for hemin and 195 W cm^{-2} for protoporphyrin.

This applies to both hemin and protoporphyrin. For comparison, the highest SNR increase from room temperature to 77 K in the spectra of hemin was observed for nominally very weak bands at 1127 cm^{-1}, 1163 cm^{-1} and 1231 cm^{-1}. Likewise, the highest SNR increase in the spectra of protoporphyrin occurred at 1227 cm^{-1}, 1125 cm^{-1} and 1479 cm^{-1}, which are very weak bands only barely visible at room temperature.

The signal increase of each band at cryogenic temperatures is quantified in percentage of the nominal room temperature signal strength in Fig. 5. The results show that while a relatively modest signal increase is possible for most bands at 173 K, Raman measurements of porphyrins at 77 K can benefit from a signal enhancement of up to 310% (hemin) and 116% (protoporphyrin). Across all resolvable bands in the spectra of hemin, a signal enhancement of 23% to 310% was observed at 77 K with most bands increasing in intensity by at least 80% and a significant number of bands increasing by more than 120%. A signal enhancement of 60% to 116% was shown across Raman bands in the spectra of protoporphyrin.

This significant signal increase and higher definition within the spectra could be very beneficial for many applications in biomedical research and diagnostics. Furthermore, decreasing the temperature of the sample is a relatively simple procedure that does not require a compromise between signal enhancement due to resonance and detectability in cases where certain spectral features can only be observed at specific excitation wavelengths. Moreover, it can be applied to any Raman instrument and excitation wavelength without any negative side effects.

In comparison, Raman signal enhancements of organic molecules by a factor of 10^7 to 10^{11} have been demonstrated using surface enhanced Raman spectroscopy (SERS).[28,29] However, despite its remarkable signal enhancement abilities, SERS has not been able to gain grounds in real world applications due to the inherent complexity of SERS implementation

and spectra reproducibility issues.[7,30] SERS spectra can be very specific to the particular SERS substrate used and its parameters, including the suitability of the SERS substrate for a given excitation wavelength and molecule size.[28] Moreover, SERS spectra can also be highly dependent on the location of the measurement within the same substrate.[29] Due to the complexity of reproducing SERS spectra with different experimental set ups as well as within the same experiment and the consequent lack of reference data, the analysis of SERS data can be too ambiguous for many applications.[7,30] As a result of this, SERS has struggled to become a widely adopted analytical technique in the industry. In comparison, cryogenic Raman measurements are a relatively effortless method of enhancing the Raman signal of porphyrin molecules, which can provide a significant signal and spectra definition enhancement without the complexity of SERS implementation and introducing potential challenges in the data analysis. As such, acquisition of Raman spectra of porphyrins and their derivatives at cryogenic temperatures can be an exceptionally effective and simple method of enhancing the Raman signal and spectra quality without introducing any additional complexity in the experiments and data analysis and regardless of the Raman instrument configuration and its excitation wavelength. This can greatly enhance the scientific output of Raman spectroscopy in biomedical research, especially in the field of diagnostics, drug design and development as well as disease monitoring and analysis.

Conclusions

The results of this study show a significant enhancement of the Raman signal and spectra quality of porphyrin molecules at cryogenic temperatures. Occurrence of bands not detectable at room temperature at the same laser power density was observed and signal enhancement of up to 310% is reported in the

spectra of hemin and 116% in the spectra of protoporphyrin IX. This thermally induced signal enhancement is independent of the excitation wavelength and as such, this study demonstrates that cryogenic Raman measurements can be a very effective method of enhancing the signal strength and quality of the spectra of porphyrins and porphyrin derivatives in contemporary biomedical research. Applications that could benefit from the enhanced signal and spectral definitions include, but are not limited to, the study of blood, hemoproteins and the oxygenation process of human erythrocyte in medical diagnostics, disease analysis and monitoring, or investigation of ligand binding mechanisms and drug interactions with healthy and diseased blood cells in drug design and development.

Conflicts of interest

There are no conflicts to declare.

Acknowledgements

References

1 A. Boffi, T. K. Das, S. Della Longa, C. Spagnuolo and D. L. Rousseau, *Biophys. J.*, 1999, **77**, 1143–1149.

2 T. Kitagawa, Y. Ozaki and Y. Kyogoku, *Adv. Biophys.*, 1978, **11**, 153–196.

3 A. Pilinkienė, E. Liutkevièius, Z. Kuodis, R. Maþeikienë, G. Niaura, I. Bachmatova and L. Marcinkevièienë, *Acta medica Lituanica*, 2005, **12**, 47–53.

4 H. Sato, H. Chiba, H. Tashiro and Y. Ozaki, *J. Biomed. Opt.*, 2001, **6**, 366–370.

5 B. Venkatesh, S. Ramasamy, M. Mylrajan, R. Asokan, P. T. Manoharan and J. M. Rifkind, *Spectrochim. Acta, Part A*, 1999, **55**, 1691–1697.

6 T. G. Spiro and T. C. Strekas, *J. Am. Chem. Soc.*, 1974, **96**, 338–345.

7 C. G. Atkins, K. Buckley, M. W. Blades and R. F. B. Turner, *Appl. Spectrosc.*, 2017, **71**, 767–793.

8 B. R. Wood, L. Hammer, L. Davis and D. McNaughton, *J. Biomed. Opt.*, 2005, **10**, 014005.

9 B. R. Wood, P. Caspers, G. J. Puppels, S. Pandiancherri and D. McNaughton, *Anal. Bioanal. Chem.*, 2007, **387**, 1691–1703.

10 D. McNaughton and B. Wood, in *Proceedings of the XIXth International Conference on Raman Spectroscopy*, CSIRO Publishing, 2004, pp. 42–47.

11 C. Tempera, R. Franco, C. Caro, V. André, P. Eaton, P. Burke and T. Hänscheid, *Malar. J.*, 2015, **14**, 403.

12 B. R. Wood, S. J. Langford, B. M. Cooke, J. Lim, F. K. Glenister, M. Duriska, J. K. Unthank and D. McNaughton, *J. Am. Chem. Soc.*, 2004, **126**, 9233–9239.

13 A. J. Hobro, A. Konishi, C. Coban and N. I. Smith, *Analyst*, 2013, **138**, 3927–3933.

14 T. Frosch, S. Koncarevic, L. Zedler, M. Schmitt, K. Schenzel, K. Becker and J. Popp, *J. Phys. Chem. B*, 2007, **111**, 11047–11056.

15 R. Dasgupta, S. Ahlawat, R. S. Verma, A. Uppal and P. K. Gupta, *J. Biomed. Opt.*, 2010, **15**, 055009–055010.

16 K. Ramser, K. Logg, M. Goksör, J. Enger, M. Käll and D. Hanstorp, *J. Biomed. Opt.*, 2004, **9**, 593.

17 Y. Ozaki, A. Mizuno, H. Sato, K. Kawauchi and S. Muraishi, *Appl. Spectrosc.*, 1992, **46**, 533–536.

18 T. Ohta, J. G. Liu, P. Nagaraju, T. Ogura and Y. Naruta, *Chem. Commun.*, 2015, **51**, 12407–12410.

19 J. F. D. Liljeblad, I. Furó and E. C. Tyrode, *Phys. Chem. Chem. Phys.*, 2017, **19**, 305–317.

20 R. W. Berg, *Appl. Spectrosc. Rev.*, 2018, **53**, 503–515.

21 S. M. Pershin, V. N. Lednev, R. N. Yulmetov, V. K. Klinkov and A. F. Bunkin, *Appl. Opt.*, 2015, **54**, 5943.

22 R. Hibbert, M. C. Price, T. M. Kinnear, M. J. Cole and M. J. Burchell, in *46th Lunar and Planetary Science Conference*, 2015.

23 L. J. Sandilands, Y. Tian, K. W. Plumb, Y. J. Kim and K. S. Burch, *Phys. Rev. Lett.*, 2015, **114**, 1–7.

24 C. Girardot, J. Kreisel, S. Pignard, N. Caillault and F. Weiss, *Phys. Rev. B: Condens. Matter Mater. Phys.*, 2008, **78**, 104101.

25 J. Haines, J. Rouquette, V. Bornand, M. Pintard, P. Papet and F. A. Gorelli, *J. Raman Spectrosc.*, 2003, **34**, 519–523.

26 G. B. B. M. Sutherland, *Proc. R. Soc. London, Ser. A*, 1933, **141**, 535–549.

27 K. Dziedzic-Kocurek, H. J. Byrne, A. Świderski and J. Stanek, *Acta Phys. Pol., A*, 2009, **115**, 552–555.

28 B. Sharma, R. R. Frontiera, A. I. Henry, E. Ringe and R. P. Van Duyne, *Mater. Today*, 2012, **15**, 16–25.

29 E. C. Le Ru, E. Blackie, M. Meyer and P. G. Etchegoint, *J. Phys. Chem. C*, 2007, **111**, 13794–13803.

30 A. Bonifacio, S. Dalla Marta, R. Spizzo, S. Cervo, A. Steffan, A. Colombatti and V. Sergo, *Anal. Bioanal. Chem.*, 2014, **406**, 2355–2365.